Electronic Supplementary Material (ESI) for ChemComm.

Cl^- modification for effective promoting photoelectrochemical water oxidation over $BiVO_4$

Zhe Li, [ab] Qiqi Zhang, [ab] Xin Chen, [ab] Fang Yang, [ab] Defa Wang, [ab] Lequan Liu, *[ab] and Jinhua Ye, [abc]

[a] TJU-NIMS International Collaboration Laboratory, Key Lab of Advanced Ceramics and Machining Technology (Ministry of Education) and Tianjin Key Laboratory of Composite and Functional Materials, School of Material Science and Engineering, Tianjin University, 92 Weijin Road, Tianjin, P. R. China.

[b] Collaborative Innovation Center of Chemical Science and Engineering (Tianjin), Tianjin 300072, P. R. China.

[c] International Center for Materials Nanoarchitectonics (WPI-MANA), National Institute for Materials Science (NIMS) 1-1 Namiki, Tsukuba, Ibaraki 3050044, Japan.

Preparation of nanoporous BVO. This method is based on the theories of predecessors. The first step was to prepare BiOI grown on the cleaned fluorine-doped tin oxide (FTO). Dissolved 30 mM $Bi(NO_3)_3$ (Aladdin, 99%) in 400 mM KI (Aladdin, 99%) aqueous solution (50 mL) to obtain an opaque red-orange solution by using dilute HNO_3 (Sinopharm, 99%) adjust the pH to 1.8 to obtain a transparent red-orange solution A. Then, 100 mM p-benzoquinone (Sinopharm, 99%) was added to absolute ethanol (20 mL) to obtain solution B. Mix A and B with vigorous stirring for a few minutes for the dark black plating solution. The FTO substrate was used as the working electrode (WE), the platinum wire was used as the counter electrode (CE), and the Ag/AgCl electrode in a saturated KCl solution was used as a reference electrode (RE) to form a 3-electrode system. Prior to electrodeposition, the FTO was blow dried with N_2. Given a constant voltage of -0.15 V vs. Ag/AgCl ($V_{Ag/AgCl}$) for 7 mins at room temperature, the obtained BiOI electrode was rinsed with deionized water and blown dry with N_2. The second step was to convert BiOI to BVO. A 200 mM solution of vanadium acetylacetonate (Aladdin, 99%) in dimethyl sulfoxide (Rionlon, 99%) was prepared, 0.2 mL was dropped on the BiOI electrode. The sample was transferred to the muffle furnace and heated to 450 °C at a rate of 2 °C /min for 2 h. The removed sample was immersed in a 1 M NaOH solution and gently stirred for 30 minutes, then washed with

deionized water to obtain a bright yellow BVO. The prepared BVO was dried in an oven at 60 °C.

Preparation of Cl-BVO. The prepared BVO were immersed in a 0.01, 0.1, 0.5, 1.0 M NH_4Cl solutions and continuously gently stirred for 6, 12, 24 h to obtain Cl-BVO with different modification condition respectively.

Characterization of the samples. The scanning electron microscope (SEM; S4800, Hitachi, Japan) and a transmission electron microscope (TEM; FEI Tecnai G2 F20, USA) was used to observe the morphology and crystal structure. X-ray diffractometer (XRD; D/MAX-2500, Rigaku, Japan) was used to detect crystal structures. The microRaman spectrometer (XploRa, HORIBA Scientific, USA) with a green laser at 532 nm recorded the Raman spectrum. Fourier transform infrared (FTIR) spectroscopy was performed using Nicolet 6700 (Thermo SCIENTIFIC, USA). The UV-Vis diffuse reflectance spectrum is based on BaSO4 and tested on a spectrophotometer with an integrating sphere accessory (Shimadzu UV-1800, Japan). X-ray photoelectron spectroscopy (XPS) measurement was performed on Escalab 250 (Thermo Scientific, USA), using monochromatic Al Kα radiation and C 1s peak (284.8 eV) as a reference. Steady-state fluorescence measurements and transient fluorescence were carried out on a fluorescence spectrophotometer (Fluorolog-3, HORIBA Scientific, USA) with an excitation wavelength of 360 nm and 390 nm, respectively.

Photoelectrochemical measurements. The photoelectrochemical (PEC) properties of the samples were tested in a three-electrode system under AM 1.5 G simulated sunlight (100 mW cm^{-2}) on working station CHI 760. The sample grown on the FTO substrate was used as the working electrode (WE), the platinum sheet was used as the counter electrode (CE), and the Ag/AgCl (saturated KCl) electrode as reference electrode. The buffer was a 0.5 M potassium borate solution (pH = 9.5). Linear scanning voltammetry tests were performed at 0.2-1.3 V vs reversible hydrogen electrode (V_{RHE}) at a rate of 20 mV/s. All potentials here were converted with the formula $E_{RHE} = E_{Ag/AgCl} + 0.197 + 0.059$ pH, where $E_{Ag/AgCl}$ was the potential obtained by Ag/AgCl reference electrode. In the presence or absence of 0.5 M Na_2SO_3, Na_2SO_3 oxidation and water oxidation are performed. The Mott-Schottky test was performed in the dark at a frequency of 1 kHz. Electrochemical impedance spectroscopy (EIS) was tested under lighting conditions at 0.7 V_{RHE}.

Theory of PEC photoelectrodes. According to previous theories, the water oxidation current density J_{H2O} is determined by the product of J_{abs}, η_{sep} and η_{trans}. When the electrolyte is changed to a buffer containing 0.5 M Na_2SO_3, η_{trans} at this time theoretically becomes 100%, thus:

$$J_{sulfite} = J_{abs} \times \eta_{sep} \quad \text{S1}$$

dividing J_{H2O} by $J_{sulfite}$ can obtain η_{trans}:

$$\eta_{trans} = J_{sulfite} / J_{H2O} \quad \text{S2}$$

The applied bias photon-to-current efficiency (ABPE) for water splitting was calculated from the following equation：

$$ABPE(\%) = \left[\frac{J(mA/cm^2) \times (1.23 - V_{bias})\ (V)}{P_{in}(mW/cm^2)}\right]_{AM\ 1.5G} \times 100\%$$

S3

Where J represents the photocurrent density given by the workstation, V_{bias} represents the given voltage, P_{in} represents the power of the solar simulator which is 100 mW/cm^2.

The incident photon-to-electron conversion efficiency (IPCE) is tested using a monochromator connected to a three-electrode system at different wavelengths, processed with the following equation:

$$IPCE(\%) = \frac{J(mA/cm^2) \times 1240}{\lambda(nm) \times P_{in}(mW/cm^2)} \times 100\%$$

S4

Where J represents the photocurrent density under monochromatic light at 1.23 V_{RHE}, λ represents the wavelength of monochromatic light, P_{in} represents the optical density.

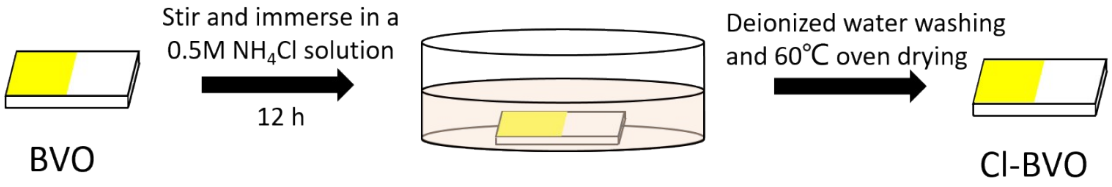

Figure S1. Schematic representation of the synthesis procedure of Cl-BVO.

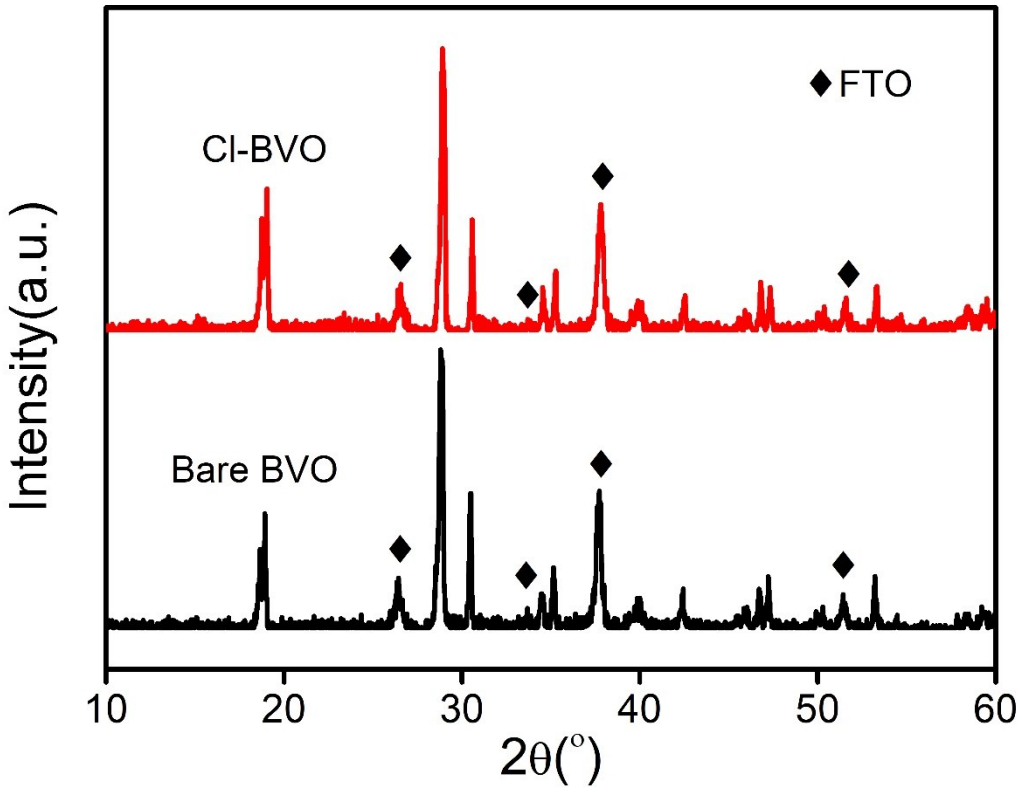

Figure S2. XRD patterns of BVO and Cl-BVO.

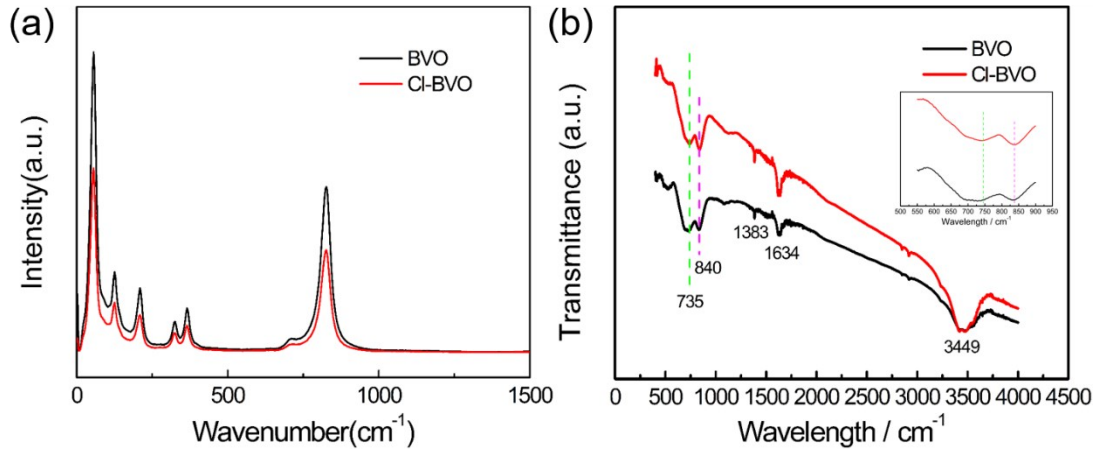

Figure S3. Raman spectroscopy (a) and Fourier-transform infrared (FTIR) spectra (b) of BVO and Cl-BVO photoanodes. The inset is an enlarged FTIR image between 500 cm^{-1} and 950 cm^{-1}.

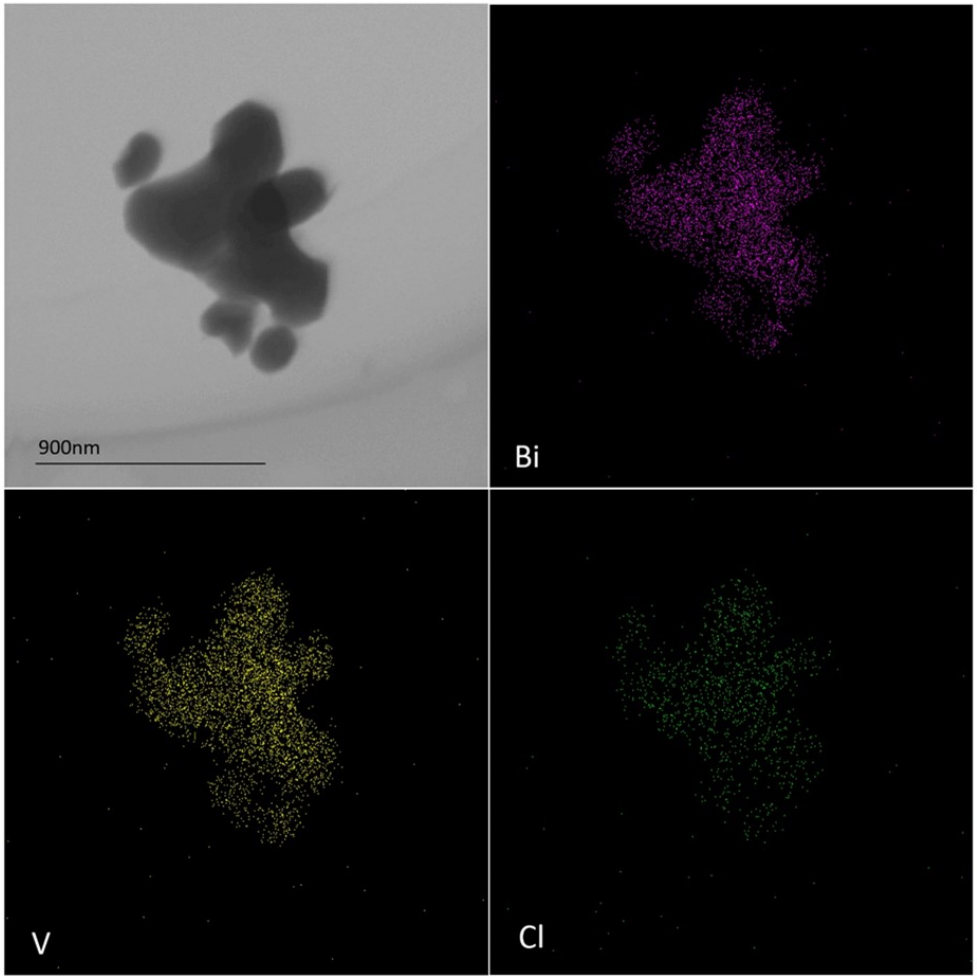

Figure S4. Elemental mapping analysis of Cl-BVO.

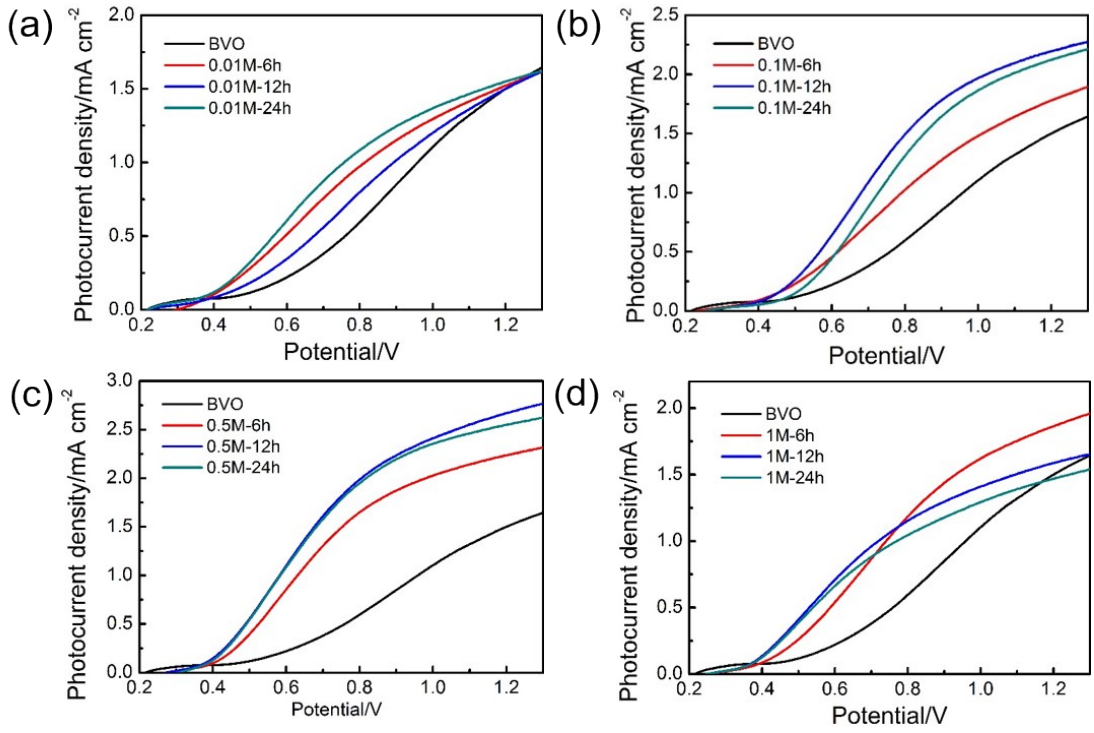

Figure S5. J-V curves of BVO treated with 0.01 M, 0.1 M, 0.5 M, 1 M NH_4Cl for 6 hours, 12 hours, and 24 hours, respectively.

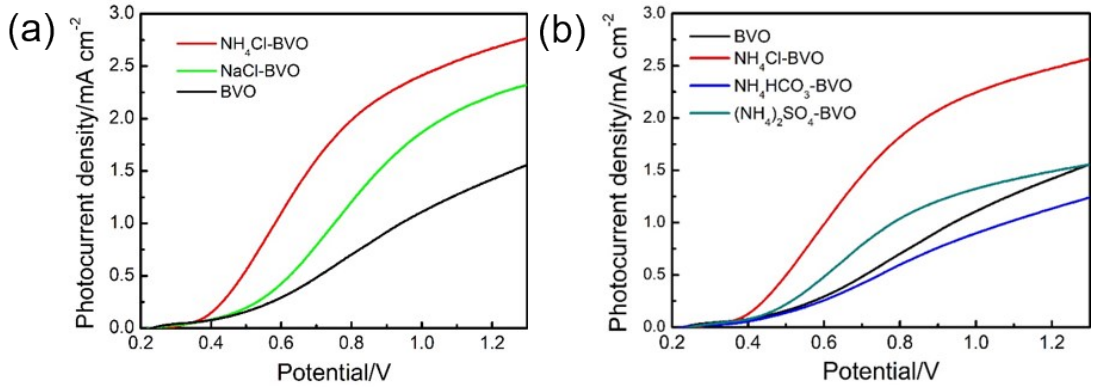

Figure S6. J-V curves of BVO treated with (a) different Cl^- solutions and (b) different NH_4^+ solutions in 0.5 M for 12 hours.

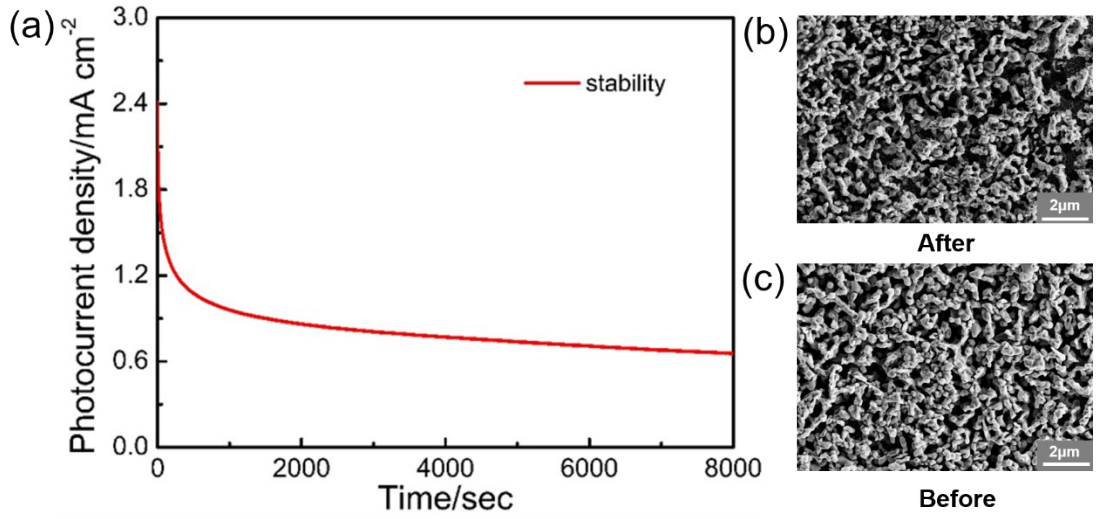

Figure S7. (a) J-t curves of Cl-BVO photoanodes measured at 1.23 V_{RHE}. SEM of Cl-BVO photoanodes before (b) and after (c) J-t tests.

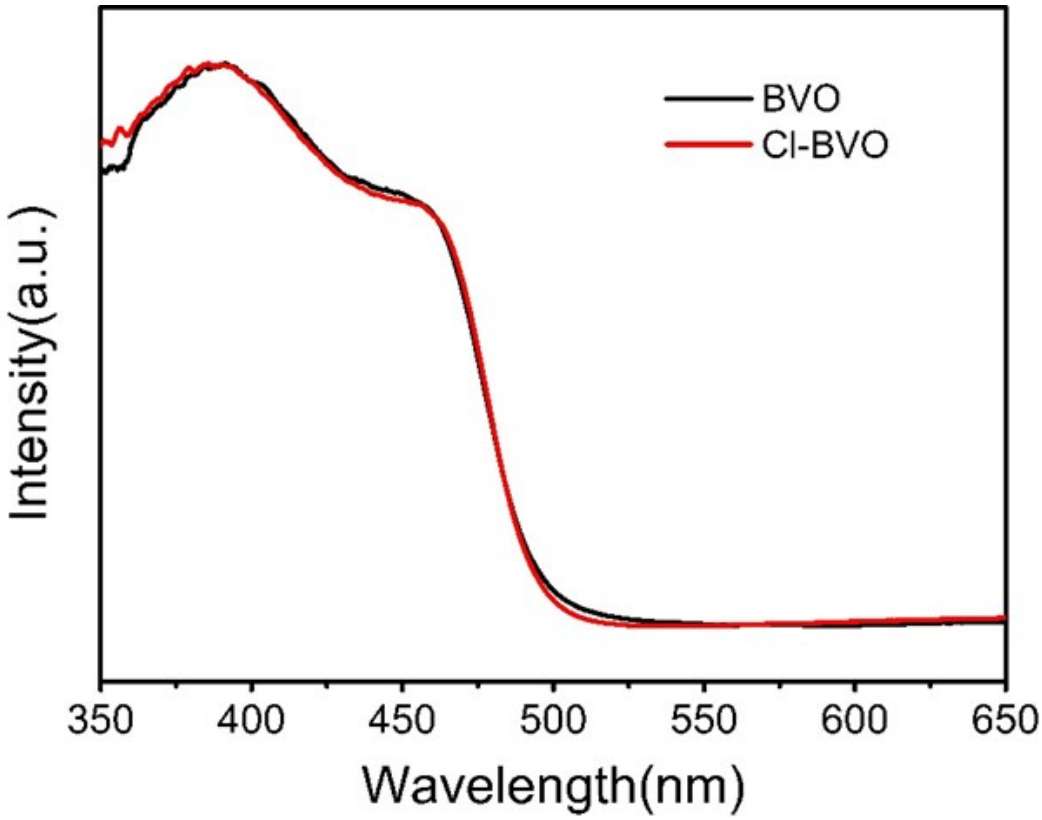

Figure S8. UV-Vis diffuse spectra of BVO and Cl-BVO photoanodes.

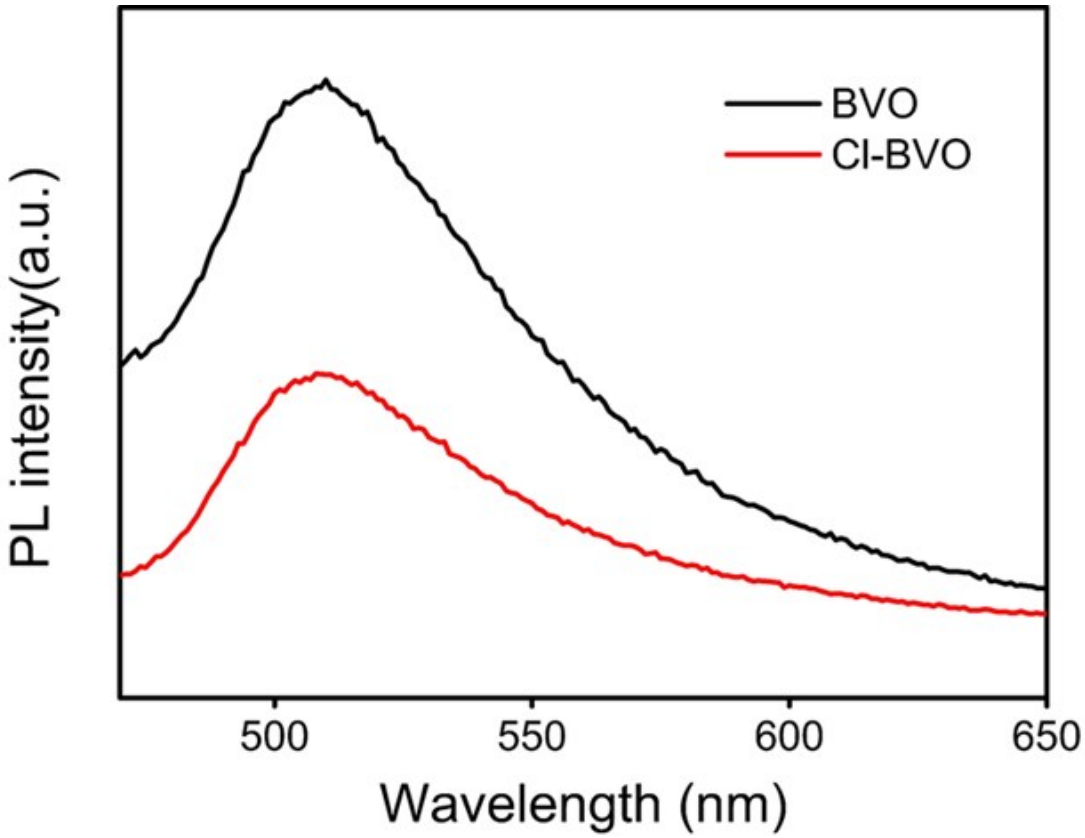

Figure S9. Steady-state fluorescence of BVO and Cl-BVO photoanodes.

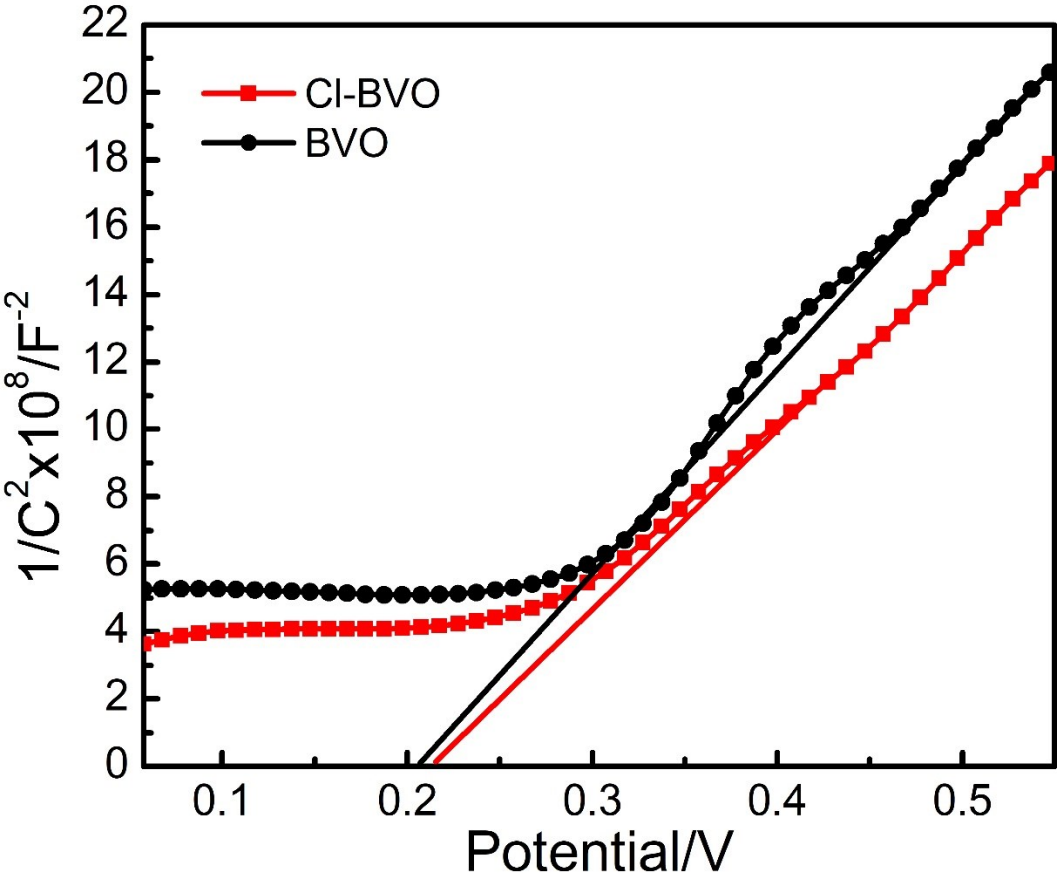

Figure S10. Mott-Schottky plots of BVO and Cl-BVO photoanodes measured in a 0.5 M borate buffer at pH 9.5 in dark.

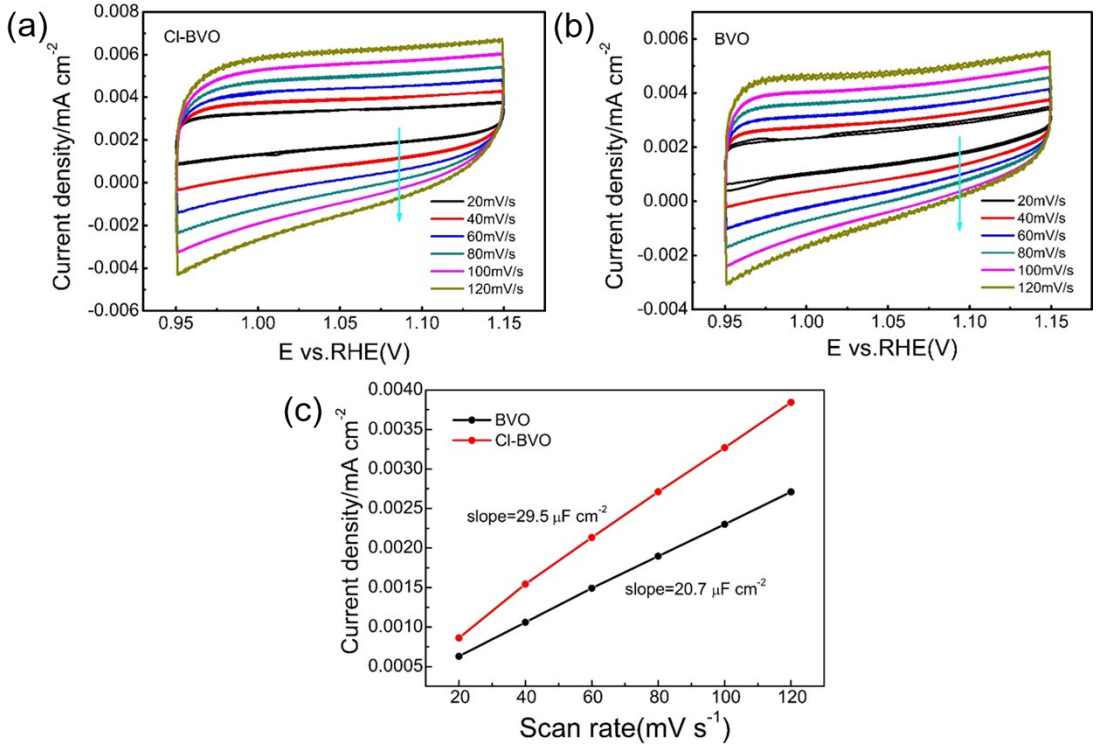

Figure S11. Cyclic voltammetry test in the dark for (a) Cl-BVO and (b) BVO at different scan rates (20, 40, 60, 80,100, and 120 mV/s) in a potential range without Faradaic processes. (c) Charging current densities recorded at 1.05 V_{RHE} at different scan rates.

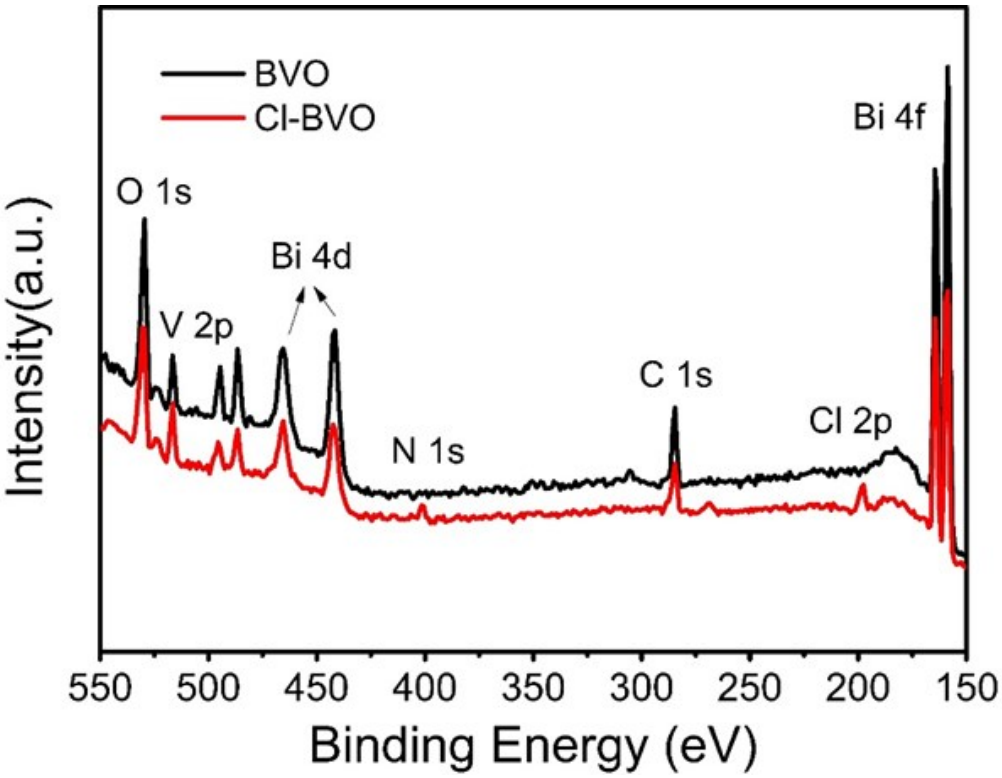

Figure S12. XPS spectra of BVO and Cl-BVO photoanodes.

Table S1. Comparisons of photocurrent activity of Cl-BVO with other reported BVO photoanodes without any co-catalyst.

Photoanodes	**J_{ph}/mA cm^{-2} (1.23 V_{RHE})**	**Onset potential (V_{RHE})**	**Electrolyte**	**Renferences**
Cl-BVO	2.7	0.38	0.5 M borate bu□er pH 9.5	This work
H-BVO	2.4*	0.5*	0.5 M Na_2SO_4 pH 6.8	1
UV curing BVO	1.2	0.42	0.1 M phosphate buffer pH 7	2
Photocharged BVO	4.3	0.25	0.1 M phosphate-borate-acetate pH 10	3
S-BVO	1.8	0.27*	0.1 M potassium buffer pH 7	4
B-BVO	3.5	0.32	0.5 M phosphate buffer pH 9.3	5
F-BVO	0.28	0.8*	0.1 M phosphate buffer pH 7.2	6
oxygen vacancies BVO	2*	0.3*	1 M borate bu□er pH 9.5	7
R-BVO	3.18	0.51	0.2 M phosphate buffer pH 7	8

*Evaluated the photocurrent density or onset potential based on the J-V curves in the corresponding paper.

1 G. Wang, Y. Ling, X. Lu, F. Qian, Y. Tong, J. Z. Zhang, V. Lordi, C. R. Leao and Y. Li, *J. Phys. Chem. C*, 2013, **117**, 10957-10964.

2 T. Li, J. He, B. Pena and C. P. Berlinguette, *Angew. Chem. Int. Ed.*, 2016, **55**, 1769-1772.

3 B. J. Trzesniewski, I. A. Digdaya, T. Nagaki, S. Ravishankar, I. Herraiz-Cardona, D. A. Vermaas, A. Longo, S. Gimenez and W. A. Smith, *Energy Environ. Sci.*, 2017, **10**, 1517-1529.

4 M. Lamers, W. Li, M. Favaro, D. E. Starr, D. Friedrich, S. Lardhi, L. Cavallo, M. Harb, R. van de

Krol, L. H. Wong and F. F. Abdi, *Chem. Mater.*, 2018, **30**, 8630-8638.

5 Q. Meng, B. Zhang, L. Fan, H. Liu, M. Valvo, K. Edström, M. Cuartero, R. D. Marco, G. A. Crespo and L. Sun, *Angew. Chem. Int. Ed.*, 2019, **131**, 19203.

6 M. Rohloff, B. Anke, O. Kasian, S. Zhang, M. Lerch, C. Scheu and A. Fischer, *ACS Appl. Mater. Interfaces*, 2019, **11**, 16430-16442.

7 S. Wang, T. He, P. Chen, A. Du, K. Ostrikov, W. Huang and L. Wang, *Adv. Mater.*, 2020, **32**, 2001385.

8 X. Yin, J. Li, L. Du, F. Zhan, K. Kawashima, W. Li, W. Qiu, Y. Liu, X. Yang, K. Wang, Y. Ning and C. B. Mullins, *ACS Appl. Energy Mater.*, 2020, **3**, 4403-4410.